# The scintillation process in xenon

*Akira Hitachi*
Waseda University, Japan

We discuss about Ar and Xe.

To understanding the scintillation process,
Information available for Xe is not sufficient.

Gas scintillation yield & decay
  Heavy ions
  Proportional scintillation
  Mixture

Liquid scintillation yield & decay
  Field effects
  Quenching
  Proportional scintillation
  Mixture

# Low pressure gas
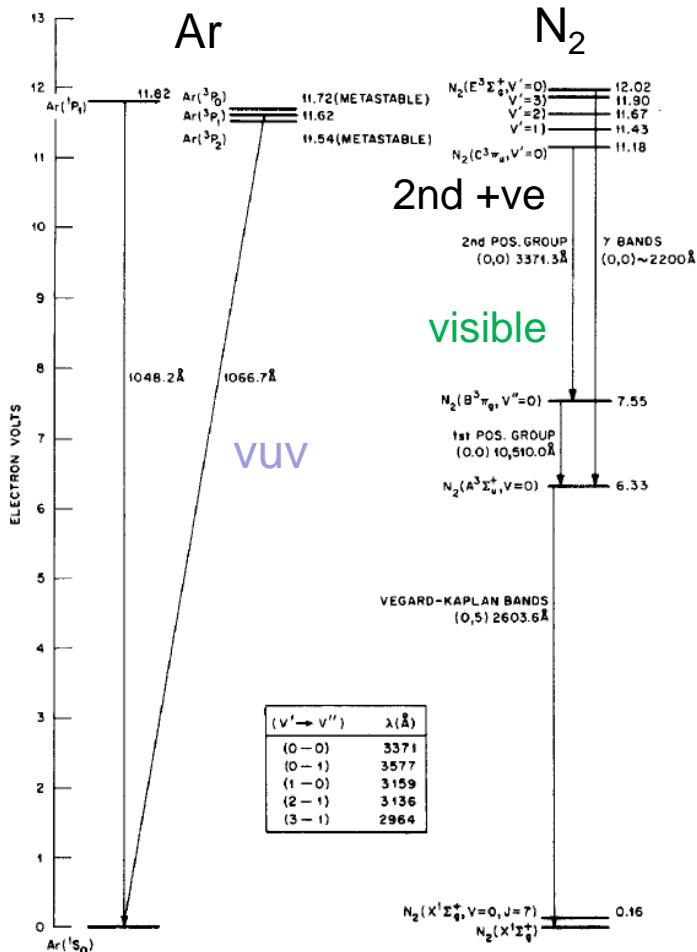


FIG. 2. Some energy levels in the argon atom and in the nitrogen molecule.

$$\dot{n}_1 = -(A_1 + a_1)n_1 + a_{21}n_2,$$

$$\dot{n}_2 = -(A_2 + a_2)n_2 + a_{12}n_1,$$
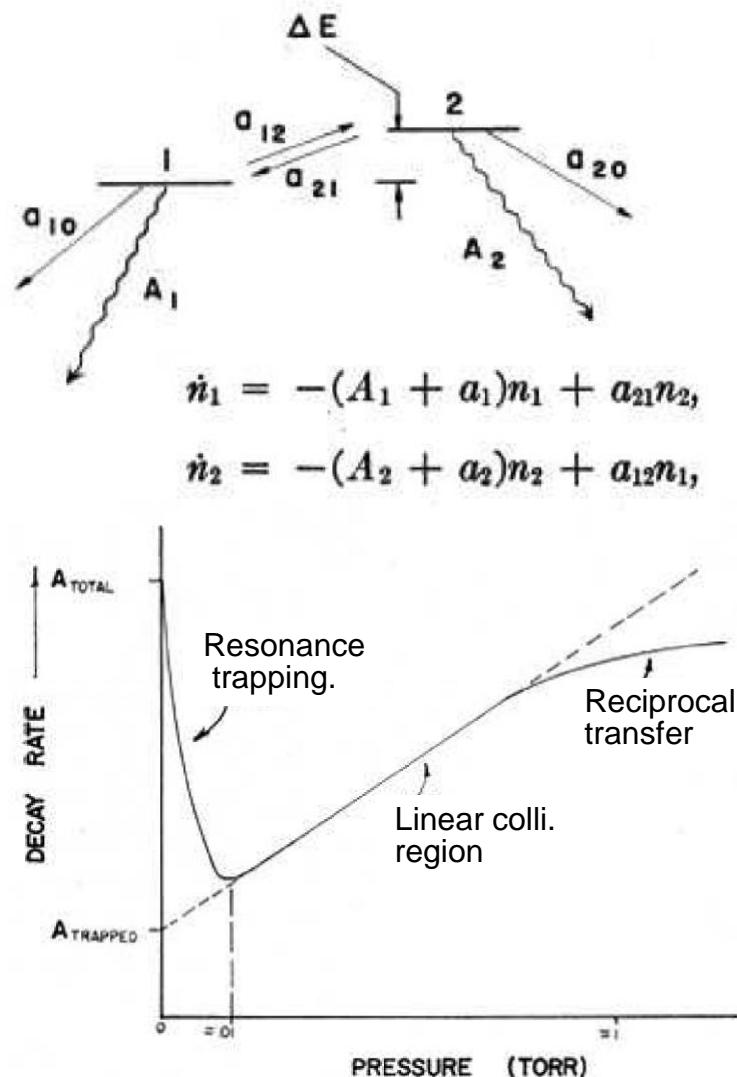
vuv → visible does not work for condensed phase

C.H.Chen, JCP 65, 1976

W. R. Bennet, Jr.,, Appl. Opt. 4 Issue S1, pp.34-57 (1965)

# Medium to high pressure gas
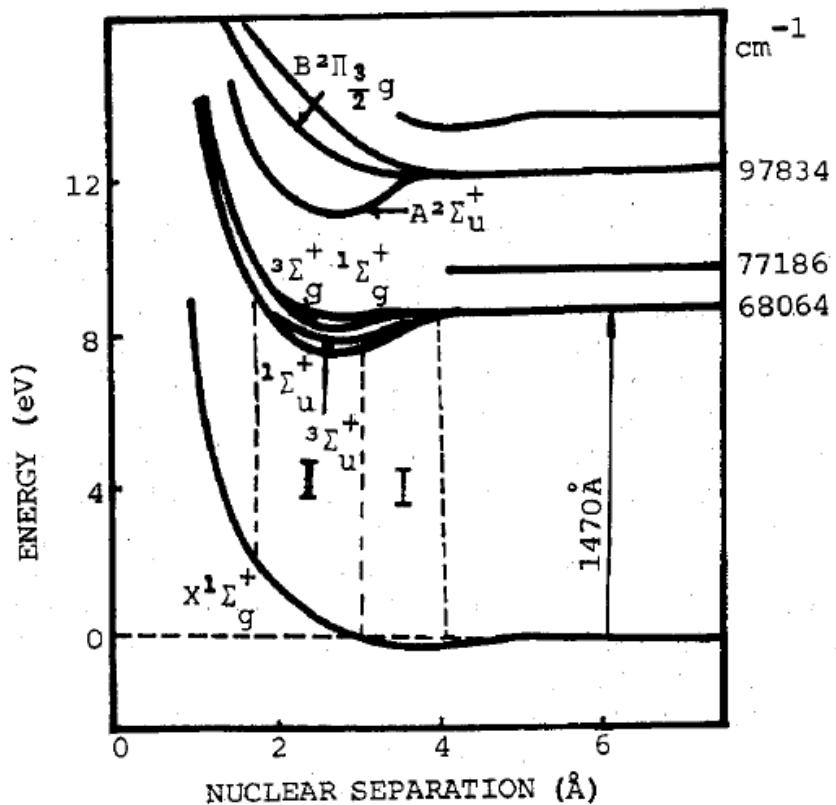


Y. Tanaka and A.S. Jursa, Appl. Opt. 50, 1118 (1960)

Good potential curves for excited Ar and Xe may be find
R.S. Mulliken, PhysRev. 1960's



$Xe_2^* \rightarrow Xe + Xe + vuv$

2nd continuum
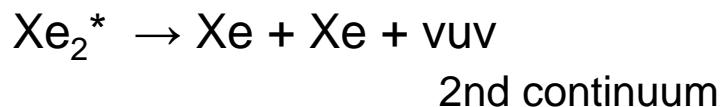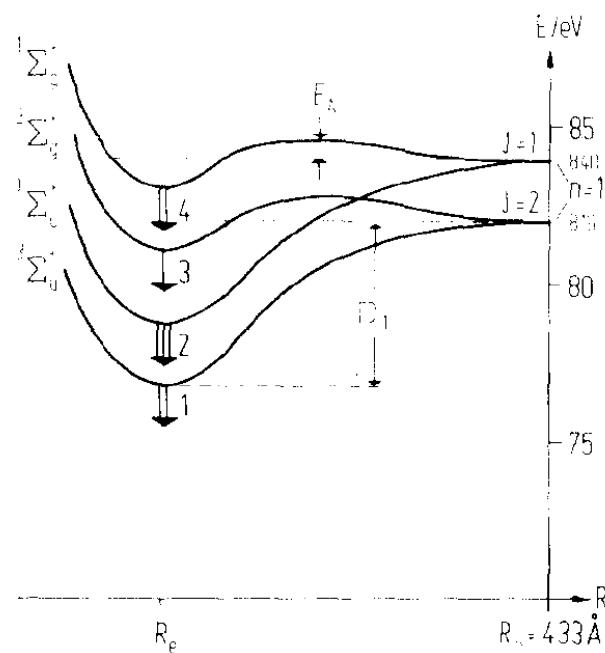
Xe is transparent for the emission
No resonance trapping.

electron excitation
$Ar_2^* \rightarrow Ar_2^{**}$   IR region
S. Arai, JCP 1970's

# Condensed phase



This part have to be reconsidered

Fig. 6.16. Relaxation cascade in the excitonic states of heavy RGS (e.g., Xe). (a) localization of free excitons; (b) electronic relaxation; (c) vibrational relaxation; (d) predissociation. The potential curves have been drawn according to the work by Molchanov /1972/ for excimer centres and Fugol /1978/ for atomic centres

b: IR emission has not been observed.

Free exciton lifetimes for Ar* and Xe* are $10^{-12}$ to $10^{-13}$ sec play important roles.

A. Hitachi
JCP

N. Schwentner, E.-E. Koch and J. Jortner, *Electronic Excitations in Condensed Rare Gases*, Springer Tracts in Modern Physics, vol. 107.

## TABLE 31.1
## Properties of LAr and LXe as Detector Media

|  |  | LAr | LXe | Comment |
|---|---|---|---|---|
| $E_g$ | eV | 14.3 | 9.28 |  |
| $W$ | eV | 23.6 | 15.6 |  |
| $W_{ph}$ | eV | 19.5 | 14 | rel. H.I. |
| $N_{ex}/N_i$ |  | 0.21 | 0.06, 0.13 |  |
| $\mu_e$ | cm$^2$/V/s | 475 | 1900 | At T.P. |
| $\mu_h$ | $10^{-3}$ cm$^2$/V/s |  | 3.5 | At T.P. |
| $D_\perp$ | cm$^2$/s | ~20 | ~80 | At 1 kV/cm |
| $\lambda$ | nm | 127 | 178 |  |
| $\tau_S$ | ns | 7 | 4.3 |  |
| $\tau_T$ | ns | 1600 | 22 |  |
| $\tau_{rec}$ |  |  | 45 | Apparent |
| $\tau_{th}$ | ns | 0.9 | 6.5 |  |
| $l_{ph}$ | cm | 66 | 29–50 |  |
| T.P. | K | 84 | 161 |  |
| $D_{self}$ | cm$^2$/s | $2.43 \times 10^{-5}$ |  |  |
| $\rho$ | g/cm$^3$ | 1.40 | 2.94 | At B.P. |
| $n$ |  |  | 1.54–1.70 |  |
| $\varepsilon_0$ |  | 1.52 | 1.94 |  |
| Radiation length[a] | cm | 14 | 2.8 | At 1 GeV |
| Moliere radius[b] | cm | 10 | 5.7 |  |

# The refractive index and attenuation length
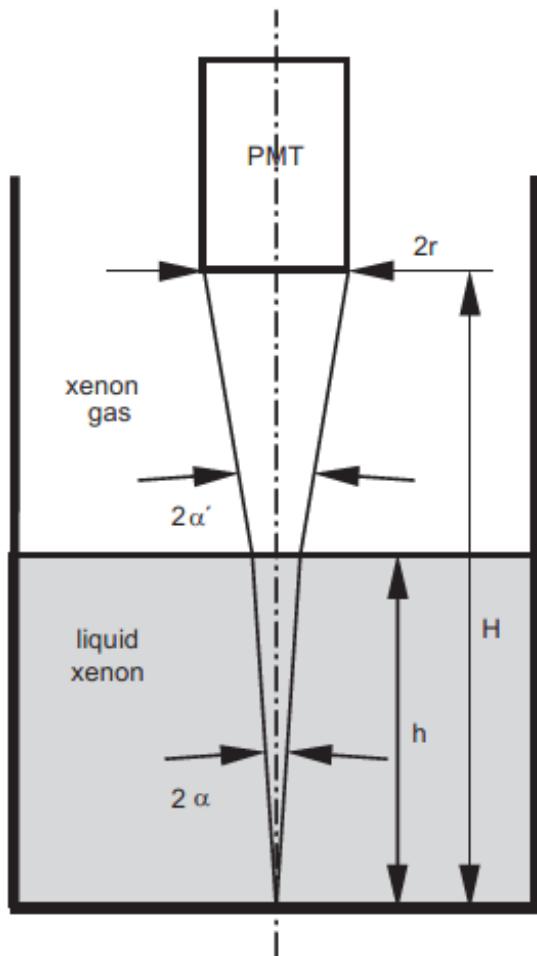


Fig. 1. Schematic drawing illustrating the principle of the experimental method.
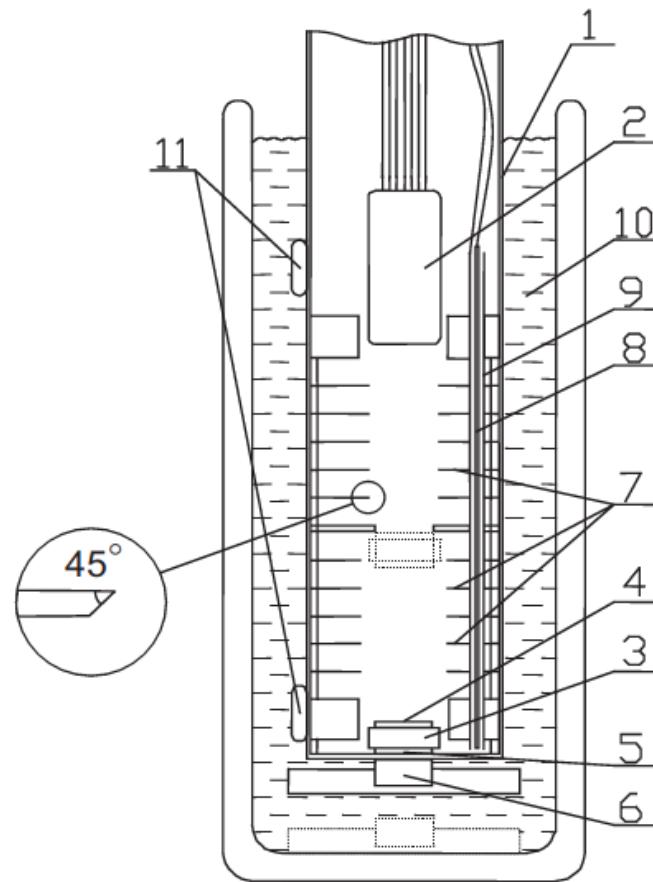


Fig. 2. Schematic drawing of the experimental set-up: 1—chamber; 2—PMT; 3,4,5—floating α-source ($^{241}$Am) assembly; 6—permanent magnet; 7—diaphragms; 8,9—level-meter; 10—alcohol cooled with liquid nitrogen; 11—thermosensors.

V.N. Solovov et al. NIMA 516 462 (2004)

Later, S. Nakamura et al. made sophisticated measurement.

**Rayleigh scattering length for liquefied rare gases**

| Liquid | Scintillation wavelength (nm) | Dielectric constant | Scattering length calculated (cm) | Scattering length measured (cm) |
|---|---|---|---|---|
| He at 4.2 K | 78 | $1.077^a$ | 600 | |
| He at 0.1 K | 78 | $1.089^a$ | $2 \times 10^4$ | |
| Neon | 80 | $1.52^b$ | 60 | |
| Argon | 128 | $1.90^b$ | 90 | $66^d$ |
| Krypton | 147 | $2.27^c$ | 60 | $82^d$, $100^e$ |
| Xenon | 174 | $2.85^c$ | 30 | $29^d$, $40^f$, $50^g$ |

**Rayleigh scattering length for mixtures of liquefied rare gases**

| Liquid | Scintillation wavelength (nm) | Dielectric constant | Scattering length calculated (cm) | Scattering length measured (cm) |
|---|---|---|---|---|
| 3% Xe in Ar | 174 | 1.29 | 280 | 170, $118^{a,b}$ |
| 3% Xe in Kr | 174 | 1.97 | 170 | $136^a$ |

measurement

$$I = I_o\, e^{-lx}$$

the inverse of the Rayleigh scattering length

$$h = \frac{\omega^4}{6\pi c^4}\left[kT\rho^2\kappa_T\left(\frac{\partial\varepsilon}{\partial\rho}\right)_T^2 + \frac{kT^2}{\rho c_v}\left(\frac{\partial\varepsilon}{\partial T}\right)_\rho^2\right]$$

# The refractive index of liquid and solid xenon

the dispersion relation

$$\frac{n^2 - 1}{n^2 + 2} = \frac{4\pi N e^2}{3m} \sum_i \frac{f_i}{\omega_i^2 - \omega^2 - i\Gamma_i\omega}$$

$f_i$ : oscillator strength
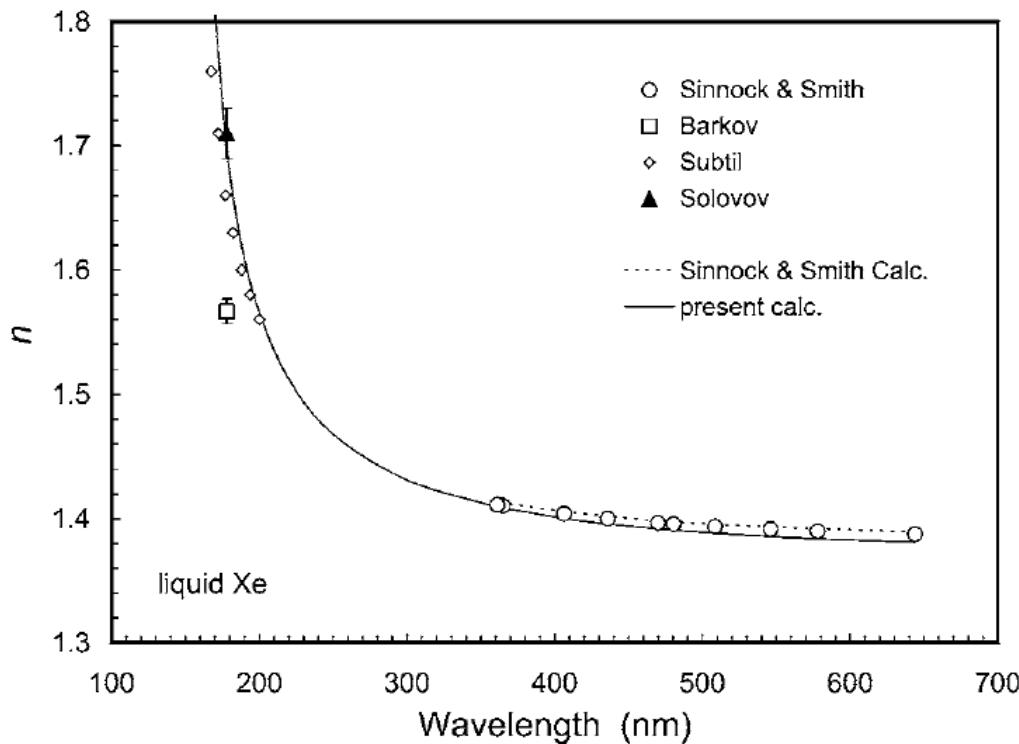


The absorption spectra in condensed xenon differ from those in gas, particularly in the vuv region. They show lines for Wanner-type "free" excitons instead of the atomic lines. We replaced $\lambda_1$ and $\lambda_2$ by two major exciton lines of liquid xenon.

$$\frac{n^2 - 1}{n^2 + 2} = 1.2055 \times 10^{-2} \frac{2}{3} \frac{N_l}{N_g} \left( \frac{0.267\,83}{43.741 - \lambda^{-2}} + \frac{0.294\,81}{57.480 - \lambda^{-2}} + \frac{5.0333}{112.74 - \lambda^{-2}} \right)$$

TABLE III. Refractive index of condensed xenon at its scintillation wavelength as well as in the uv and the visible regions.

| State | $T$ (K) | Experimental or calculated | Wavelength (nm) | | | | | | | Ref. |
|---|---|---|---|---|---|---|---|---|---|---|
| | | | Xe[a] | 188 | 200 | 361.2 | 435.8 | 546.1 | 643.9 | |
| Liquid | 170 | Expt. | 1.69 | | | | | | | 7 |
| | | Calc. | 1.68 | | | | | | | p.w.[b] |
| | 163.2 | Expt. | 1.66 | 1.60 | 1.56 | | | | | 5 |
| | 161.35 (TP) | Expt. | 1.5655 | | | | | | | 6 |
| | | Expt. | | | | 1.4111 | 1.4001 | 1.3918 | 1.3876 | 9 |
| | | Calc. | 1.70 | 1.62 | 1.566 | 1.4094 | 1.3958 | 1.3857 | 1.3810 | p.w.[b] |
| | | Calc. | | | | 1.4137 | 1.4019 | 1.3934 | 1.3896 | 9[c] |
| | | Calc. | 1.59 | | | | | | | 32 |
| Solid | 161.2 | Expt. | 1.79 | 1.69 | 1.65 | | | | | 5 |
| | 161.35 (TP) | Expt. | | | | 1.4747 | 1.4608 | 1.4507 | 1.4461 | 9 |
| | 161.35 (TP) | Calc. | 1.90 | 1.73 | 1.662 | 1.4765 | 1.4603 | 1.4484 | 1.4427 | p.w.[d] |
| | 150 | Expt. | | | | 1.4805 | 1.4667 | 1.4566 | 1.4520 | 9 |
| | | Calc. | 1.93 | | | 1.4847 | 1.4682 | 1.4560 | 1.4502 | p.w.[e] |
| | 130 | Expt. | | | | 1.4901 | 1.4763 | 1.4662 | 1.4616 | 9 |
| | | Calc. | 1.93 | | | 1.4946 | 1.4778 | 1.4654 | 1.4596 | p.w.[f] |

[a]Xenon scintillation: $\lambda = 178$ nm (for liquid) and $\lambda = 172$ nm (for solid) from Ref. 3.
[b]The average value for each exciton energy was used (see Table I).
[c]Values calculated using the tight-binding exciton model with the parameters listed in Table VII of Ref. 9.
[d]Exciton energies at 161.2 K from Ref. 5.
[e]Exciton energies at 155 K from Ref. 25.
[f]Exciton energies at 130 K from Ref. 25.

# Scintillation efficiency for LAr and LXe - LET
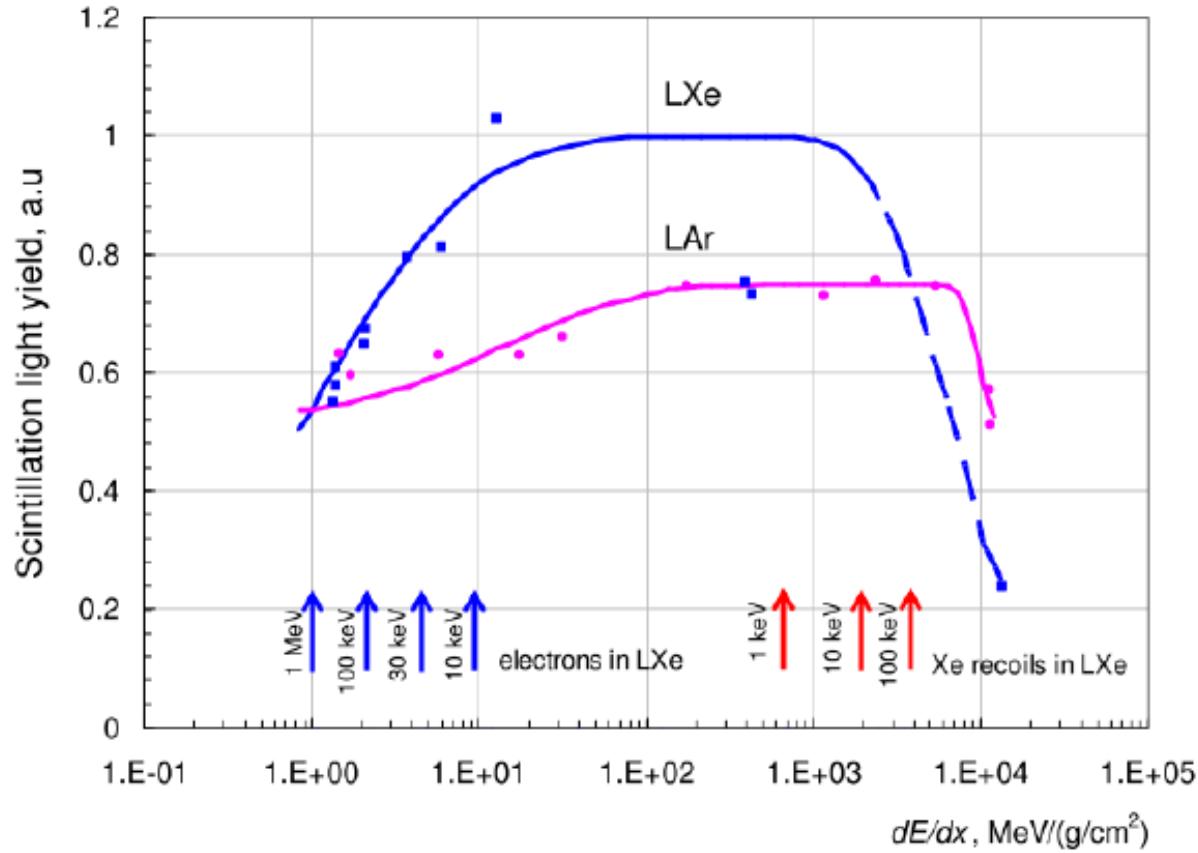


Figure 8: Relative scintillation yield of LXe and LAr as a function of linear energy transfer. Solid lines and data points are after [70]; blue arrows indicate dE/dx values for electrons in Xe computed with ESTAR [71], red ones are for Xe recoils with SRIM [59]. Vitaly&Araujo

At Low LET
Existence of escape electrons

At high LET
Scintillation quenching

High pressure

$W_s$: energy required to produce a photon



Xe Scintillation
α-excitation

This work
Dolgoshein et al.
Bolotnikov and Ramsey
Saito et al.
Kobayashi et al.
Mimura et al.

Kusano, NIMA683, 40 (2012)



Total luminescence (zero electric field)

Recombination luminescence

Excitation luminescence (0.4 Td)

Xe 0.054 g/cm³
α excitation
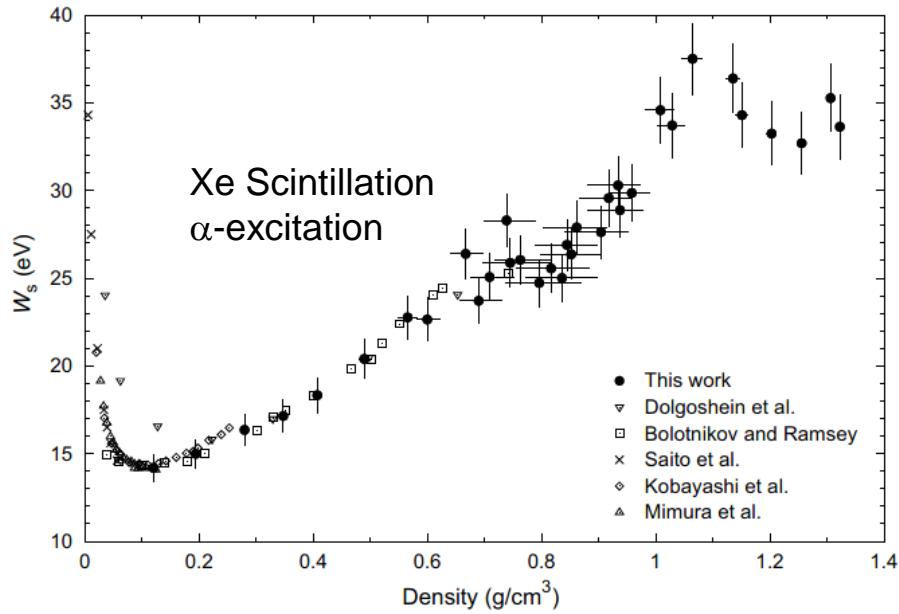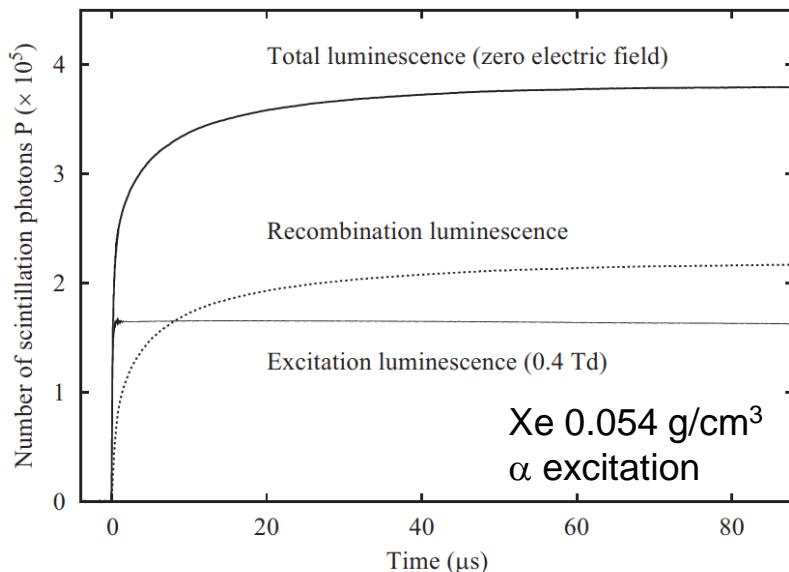
M. Mimura, NIMA 613, 106 (2010)

Excitation luminescence represent
decay times for $^1\Sigma_u^+$ and $^3\Sigma_u^+$.

$N_{ex}/N_i = 0.4$

Not true metastable
for heavy atoms

## Photon and electron multiplication

Photon and electron multiplication is possible for Ar and Xe.

Photon multiplication emission is from excimer

$$R_2^* \rightarrow R + R + h\nu \text{ (vuv)}$$ 
 M. Suzuki & S. Kubota, NIM 1970's 80's

At the electron multiplication region,

$$R_2^{**} \rightarrow R_2^* + h\nu \text{ (IR)}$$
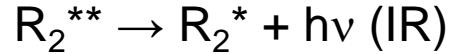
may be possible in gas.

# liquid Xe
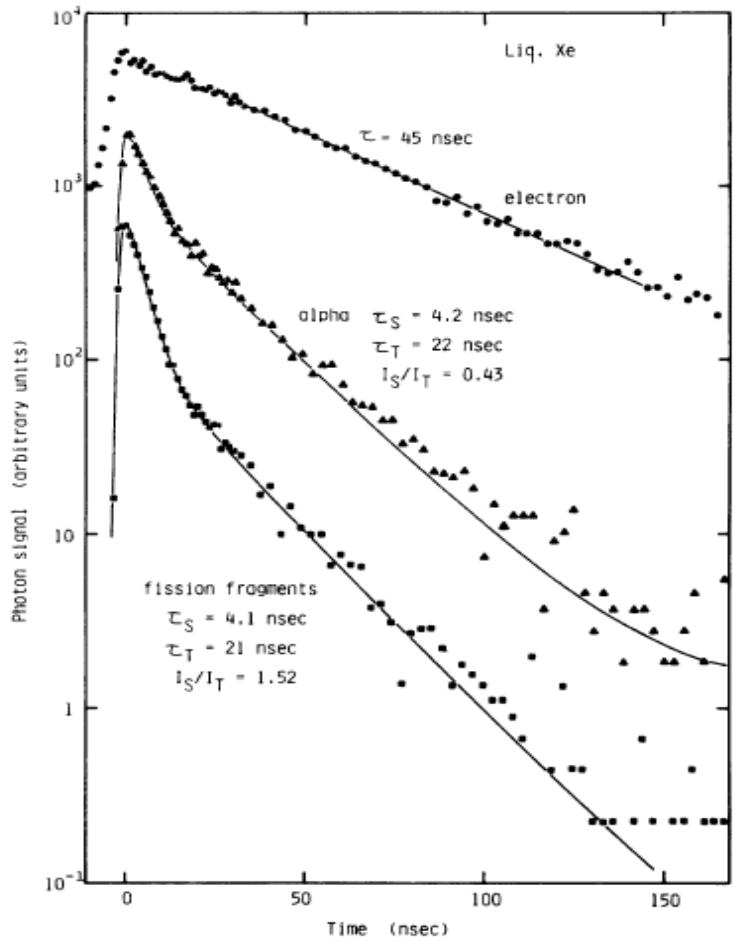


FIG. 4. Decay curves obtained for the luminescence from liquid xenon excited by electrons (●), α particles (▲), and fission fragments (■).

Liq. Xe

τ = 45 nsec

electron

alpha $\tau_S$ = 4.2 nsec
$\tau_T$ = 22 nsec
$I_S/I_T$ = 0.43

fission fragments
$\tau_S$ = 4.1 nsec
$\tau_T$ = 21 nsec
$I_S/I_T$ = 1.52



Liq. Xe
electron

FIG. 5. Variation of $I^{-1/2}$, where $I$ is the luminescence intensity, as a function of time obtained under electron excitation for liquid xenon. See Ref. 19.

The decay for electrons in LXe is due to recombination light.

The emission lifetimes for $R_2^*$ do not depend on LET.
$R_2^*$ are not responsible for quenching
Quenching occurs much faster.

A. Hitachi et al, PRB 27, 5279 (1983)

# Decay Times in LXe

**TABLE II.** Decay times for the fast $\tau_S$ and the slow $\tau_T$ components of luminescence from liquid xenon. The intensity ratios $I_S/I_T$ of the fast component to the slow component are also shown. FF stands for fission fragments. All decay times are in nsec.

| Particle | $\tau_S$ | $\tau_T$ | $I_S/I_T$ | Reference |
|---|---|---|---|---|
| Electron | | $34\pm2$ | | Kubota et al.[a] |
| | $(2.2\pm0.3)$ | $(27\pm1)$ | $(0.05)$ | $(E=4$ kV/cm$)$[a] |
| | | $32\pm2$ | | Keto et al.[b] |
| | | $45$[c] | | This work |
| | | recombination | | |
| $\alpha$ | $3$ | $22$ | $1.5$[d] | Kubota et al.[e] |
| | $4.3\pm0.6$ | $22\pm1.5$ | $0.45\pm0.07$ | This work |
| FF | $4.3\pm0.5$ | $21\pm2$ | $1.6\pm0.2$ | This work |

[a]Reference 13.
[b]Reference 16.
[c]Apparent decay time for times 30—150 nsec after the peak of luminescence; this component does not necessarily represent the decay for $^3\Sigma_u^+$.
[d]This value is obtained from the amplitude ratio quoted in Ref. 20.
[e]Reference 20.

Scintillation yields for e and $\gamma$ in LXe



B. Yang @JPS 2017

Liquid Xe

XMASS
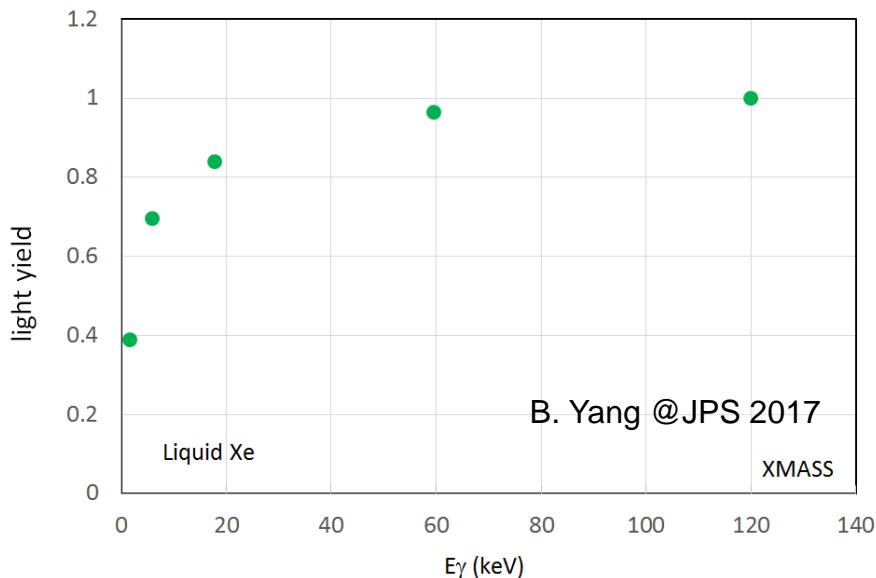
Decay time of slow component for electrons and $\gamma$-rays recombination
Approximated as an exponential decay



H. Takiya et al. NIMA 834 192 (2016)
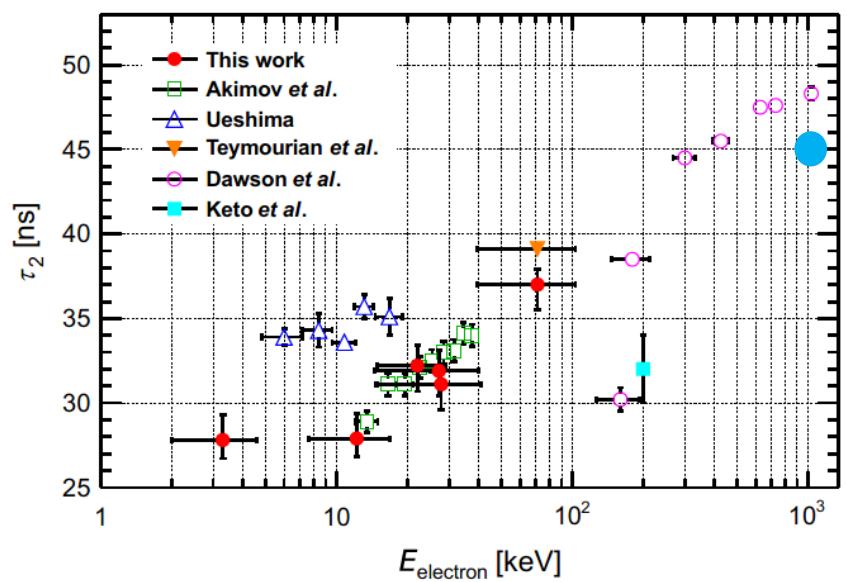
| projectile | $\tau_s$ [ns] | $\tau_t$ [ns] | $\frac{I_s}{I_t}$ | Ref. |
|:---:|:---:|:---:|:---:|:---:|
| $^{32}$S | $6.47 \pm 0.09$ | $1224.0 \pm 17.9$ | $2.19 \pm 0.07$ | (1) |
| $p^+$ | $3.20 \pm 0.02$ | $1355.8 \pm 5.8$ | $0.28 \pm 0.01$ | (1) |
| $e^-$ | $<6.2$ | $1300 \pm 60$ | $0.51 \pm 0.05$ | (2) |

$$\frac{I_s}{I_t} = \frac{\int_0^\infty A_s \cdot \exp\{-\frac{t}{\tau_s}\}dt}{\int_0^\infty A_t \cdot \exp\{-\frac{t}{\tau_t}\}dt}$$

(1) Hofmann et al. Eur. Phys. C (2013) **73**:2618
(2) Heindl et al. EPL, **91** (2010) 62002

A. Neumeier

2. Continuum

Xe

| | Sulfur |
| | Proton |
| | Gold |

Counts

Wavelength [nm]

Hofmann et al. Eur. Phys. C (2013) **73**:2618



counts

time [ns]

counts

time [ns]

proton beam

sulfur beam
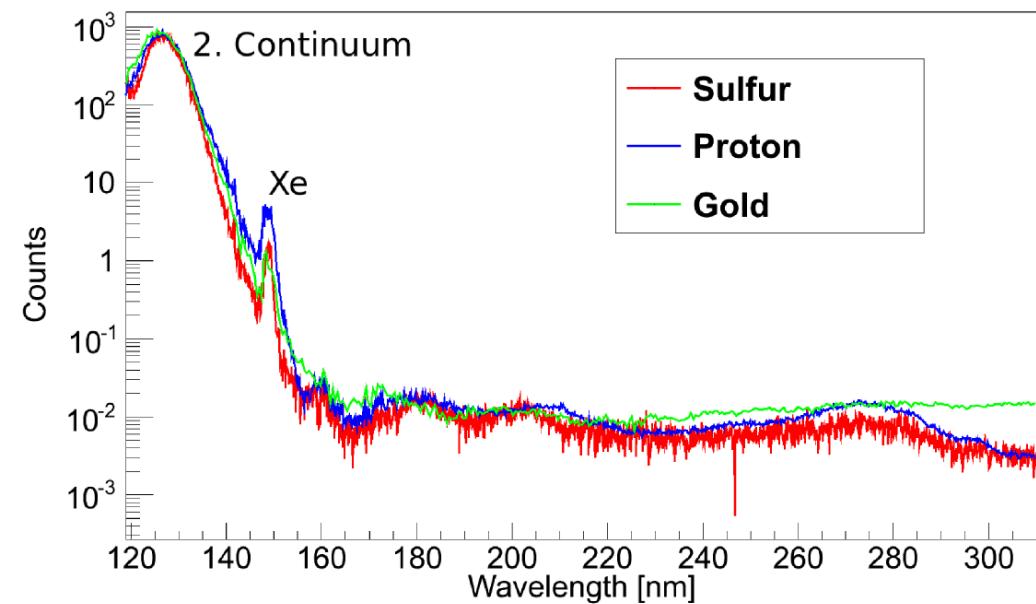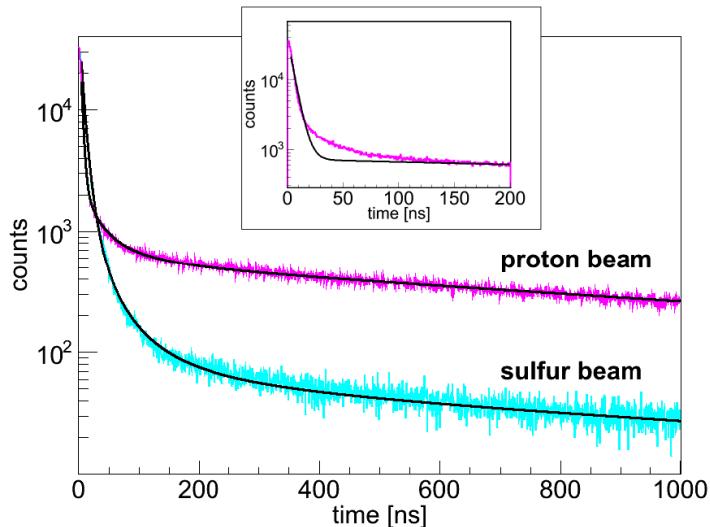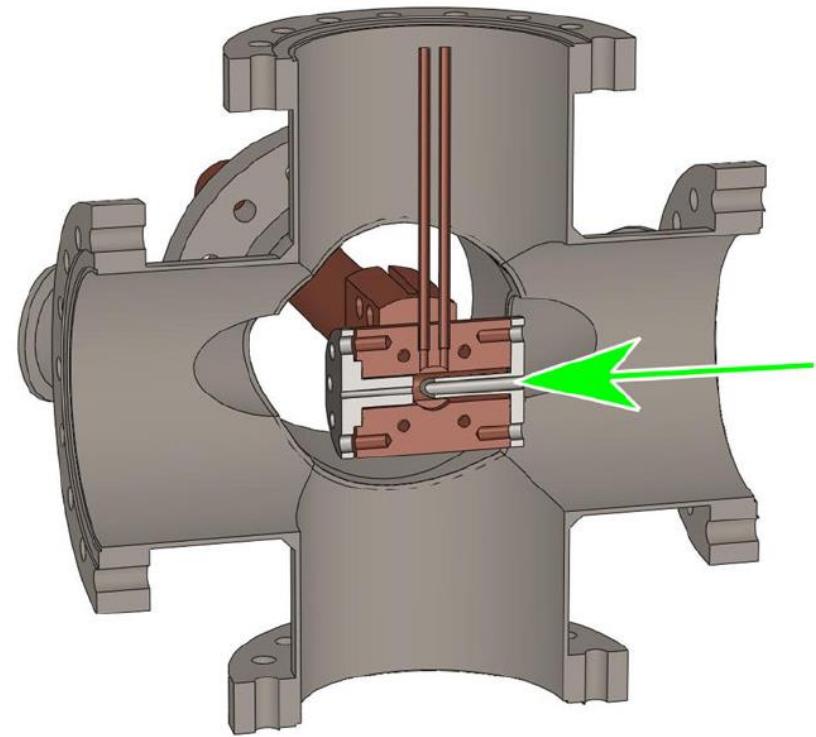
Fitting for two or more exponential is quite difficult.
A method is fit it after Fourier transformation.

Hofmann et al. Eur. Phys. C (2013) **73**:2618

# Field dependence on Scitillation & Charge in LXe - Electrons
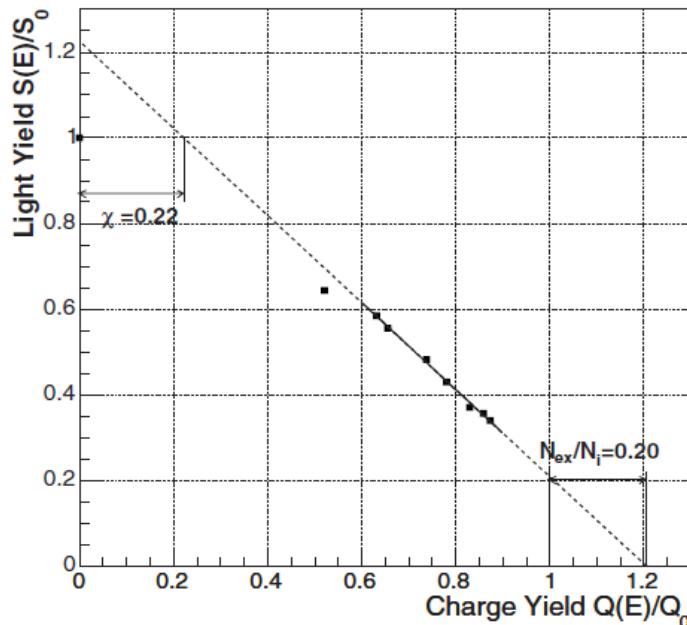


FIG. 4. Correlation between light yields and charge yield for 662 keV γ rays.



PHYSICAL REVIEW B **76**, 014115 (2007)

XENON
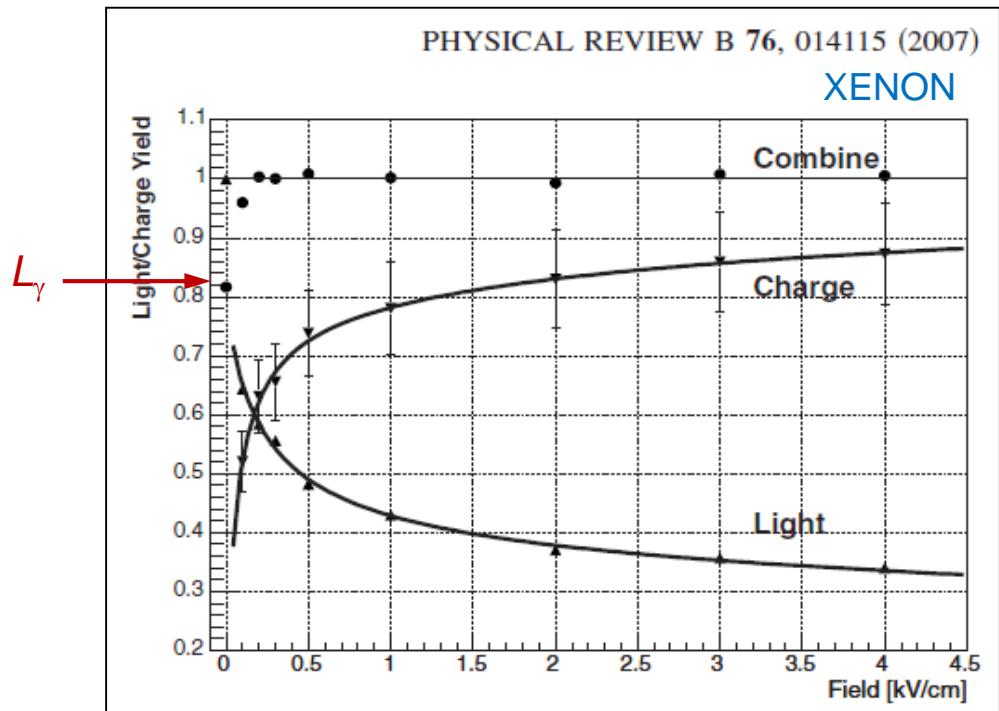


*S* and *Q* are complementary to each other

$Q + aS = \text{const.}$

$$\frac{S}{S_0{}'} = \frac{1 + N_{ex}/N_i - Q/Q_\infty}{1 + N_{ex}/N_i - \chi}$$

↑
escape electrons
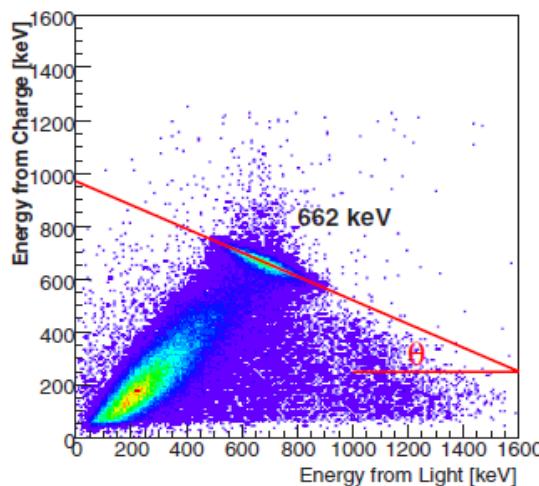
This relation can be used to obtain $L\gamma$

# $\alpha$-particles and fission fragments in LAr
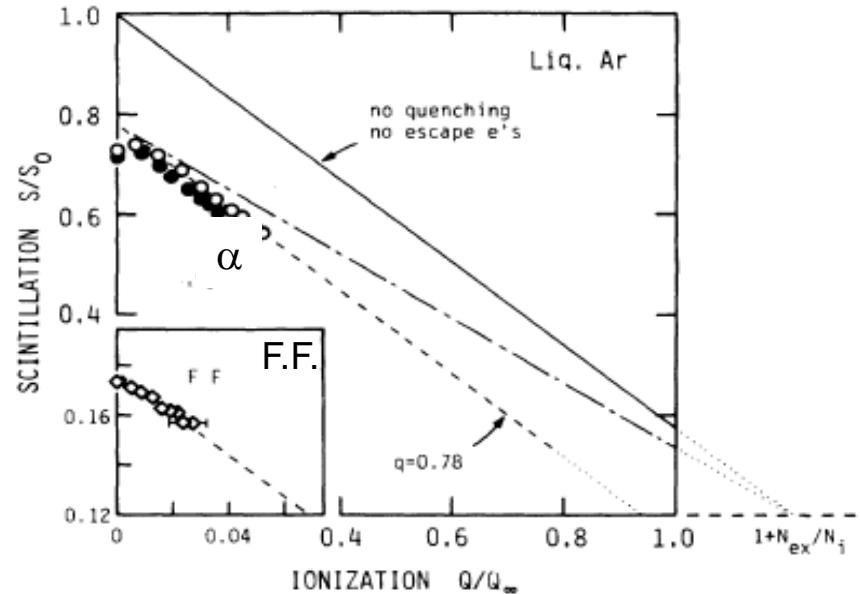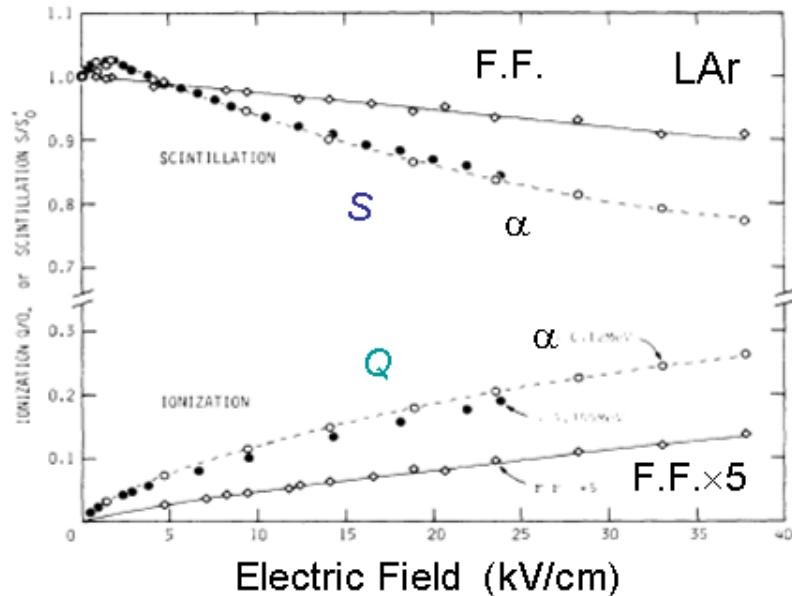


$$N_i + N_{ex} = (q\phi_{vuv})^{-1}S_0' \quad \text{for } E = 0 \ ,$$

$$N_i + N_{ex} = q^{-1}Q + (q\phi_{vuv})^{-1}S \quad \text{for } E \neq 0 \ ,$$

$$\frac{S}{S_0} = \frac{q(1 + N_{ex}/N_i) - Q/Q_\infty}{1 + N_{ex}/N_i}$$

$N_{ex}/N_i = 0.21$

Hitachi et al. PRA 35, 3956 (1987)

# Heavy ion track

The maximum impact parameter $b_{max}$ is given by Bohr's impulse principle

$$\frac{2b_{max}}{v} \cdot E_1 \geq \hbar \qquad (\beta \ll 1)$$

$v$: the incident ion velocity
$E_1$ : the lowest excitation energy.

The cylindrical field caused by positive charges on track axis $\implies$ No escaping electrons

δ-ray    penumbra

$b_{max}$
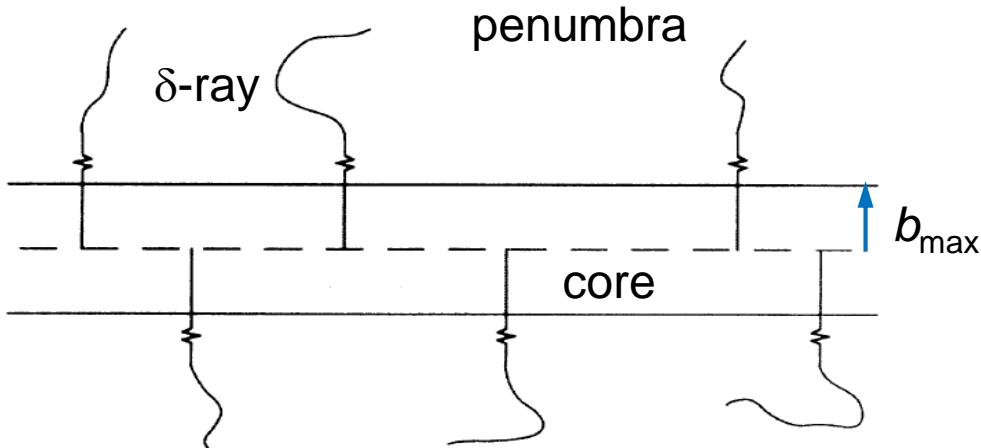
core

Quenching occurs in the core.
The energy $T_s$ available for scintillation is

$$T_s = qT = q_c T_c + T_p$$

For α-particle, $T_c/T = 0.72$
the experimental $q = 0.71$ in LAr,

$$T_s/T = 0.71 = 0.72 q_c + 0.28$$

$$q_c = 0.6$$

For relativistic ions, $T_c/T \approx 0.5$

For recoil ions,
$T_c/T = 1$
$b_{max} \approx a_0$ : atom distance

Stopping power theory tells equipartition of glancing and distant collisions

# Quenching calculation for rare gas liquids I
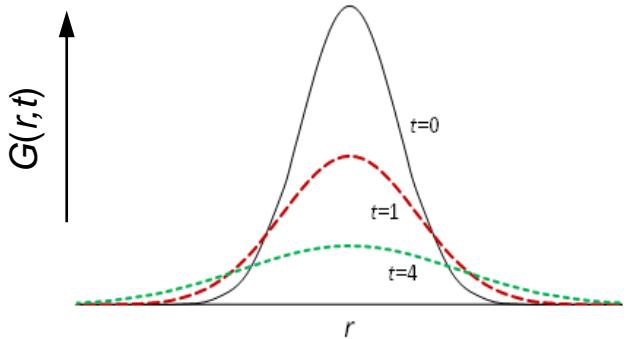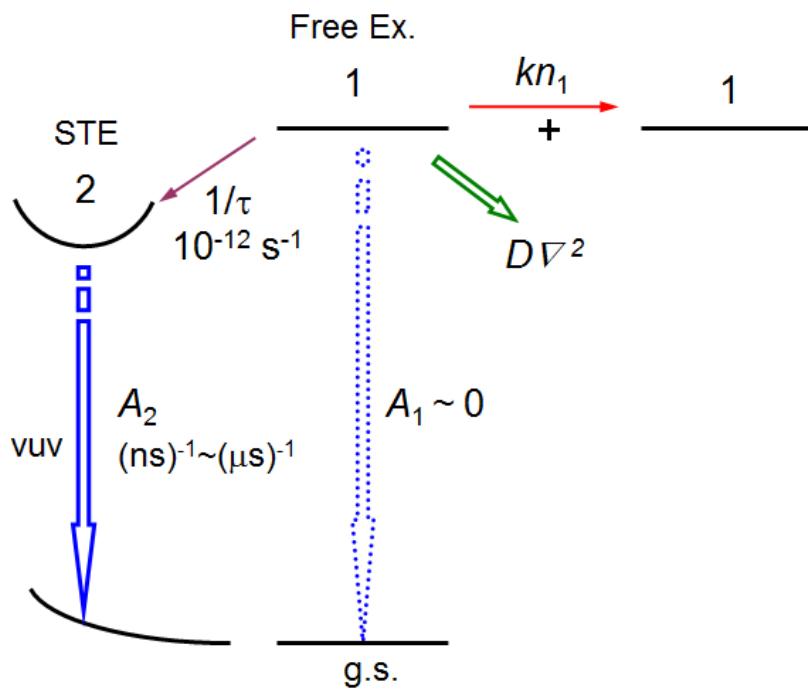
Exciton-exciton collisions.

$$R* + R* \rightarrow R + R^+ + e^-(KE)$$
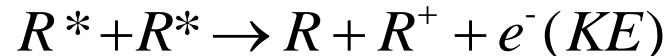
$e^-$ loses *KE* before recombination

Rate equations

$$\begin{cases} \partial n_1/\partial t = D\nabla^2 n_1 - kn_1^2 - n_1/\tau - A_1 n_1 \quad (1) \\ \partial n_2/\partial t = n_1/\tau - A_2 n_2 \end{cases}$$

(with $A_1 n_1 \to 0$ and $A_2 n_2 \to 0$ marked)   (2)

"prescribed diffusion" in cylindrical geometry

$$n_1(r,t) = N(t)G(r,t)$$

$$G(r,t) = (\pi a_1^2)^{-1} \exp(-r^2/a_1^2) \quad \text{Gaussian}$$

$$a_t^2 = a_0^2 + 4Dt \quad \text{normalized}$$

*N(t)*: no. of excited species per unit length

$$N_0 = LET \cdot T_c/T \cdot \rho \cdot (1 + N_{ex}/N_i)/W$$

$D = 1$ cm$^2$/s     $m_{ex} = 0.5 m_e$

Rate parameters:

$\tau \sim 10^{-12}$ s

$k = \sigma v$

$\sigma$: the cross section $= \sigma_{HS}/4 \sim 170/4$ Å$^2$

*v*: the collision velocity  $1.2 \times 10^7$ cm/s

**Free Ex.**  1  $\xrightarrow{kn_1}$  1  +

STE  2  $1/\tau$  $10^{-12}$ s$^{-1}$  $D\nabla^2$

$A_2$  (ns)$^{-1} \sim (\mu s)^{-1}$  $A_1 \sim 0$

vuv

g.s.

$G(r,t)$   $t=0$   $t=1$   $t=4$   $r$

A. Hitachi, A. Mozumder, and T. Doke, PRB 1992

# Quenching calculation for rare gas liquids II

$$\partial n_2 / \partial t = n_1 / \tau - A_2 n_2 \qquad (2)$$

$$N_2(t) = \int_0^t \frac{N(t')}{\tau} dt'$$

$$q_c = N_2(\infty) / N_0 = \int_0^\infty \frac{N(t')}{\tau} dt' / N_0$$



$$T_s = qT = q_c T_c + T_p$$
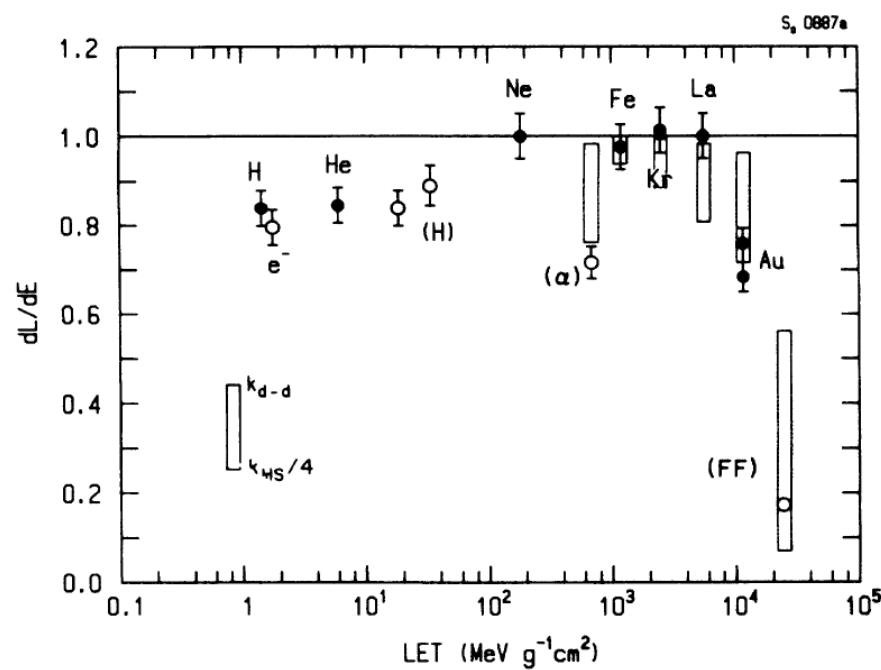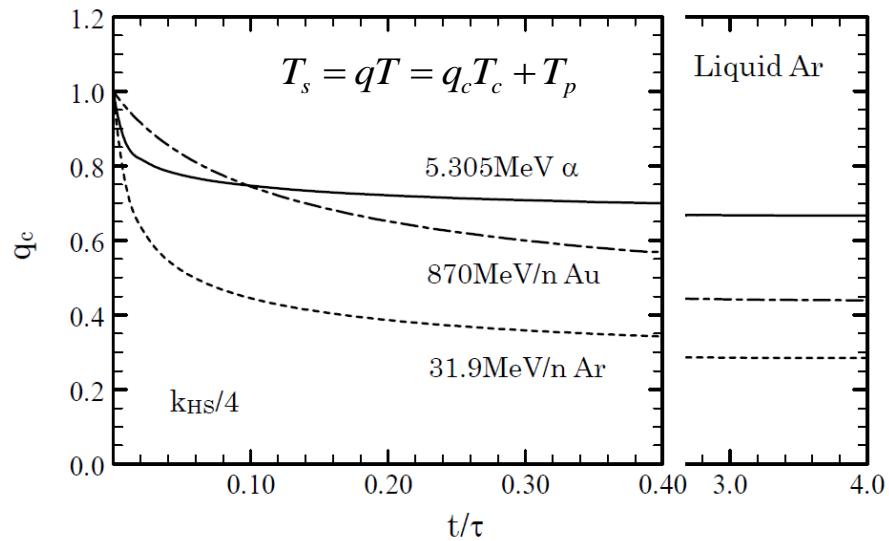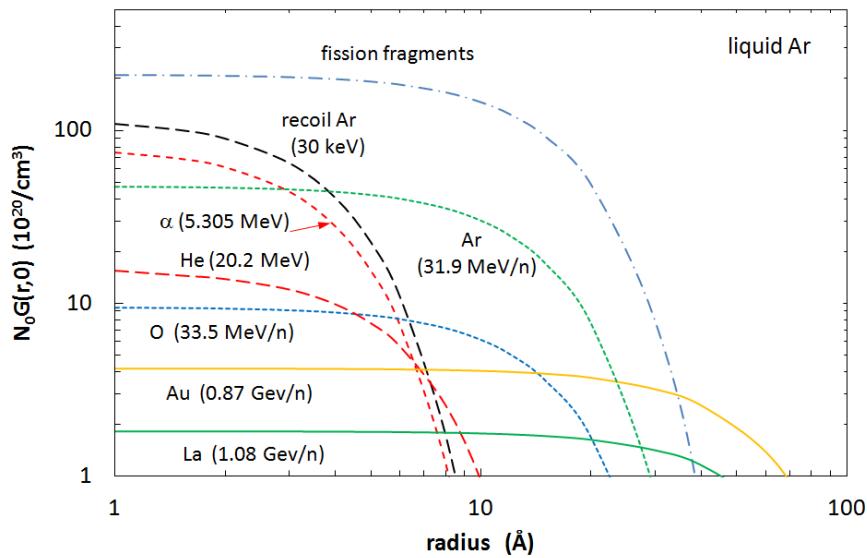
## Mixture   Energy levels

Due to formation of valence band. The gap energy $E_g$ is less than ionization energy $I$. The ionization threshold $I_s$ of a molecule is reduced in solution.

$$I_s = IP + P_+ + V_0$$

Polarization energy $P_+$ of the positive ions is given by the Born equation;

$$P_+ = -\frac{e^2}{2r_+}(1-\varepsilon^{-1})$$

$V_0 = -0.17\text{eV (Ar)}, -0.65\text{eV (Xe)}$

The energy of the quasifree electron at the bottom of conduction band.

$$R_2^* \rightarrow R + R + h\nu$$

$R^* + X \rightarrow R + X^+ + e^-$

$R_2^* + M \rightarrow R + R + M^+ + e^-$
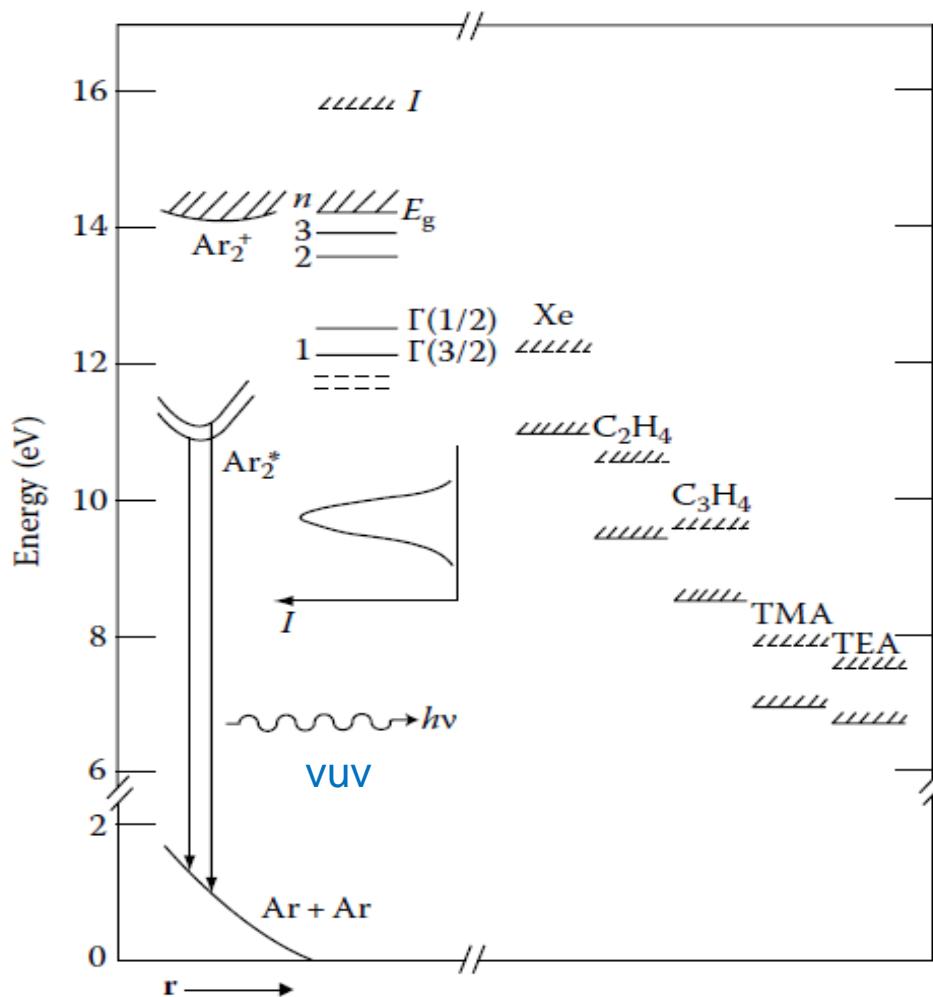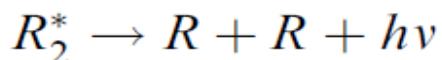


**FIGURE 31.1**   Schematic diagram for condensed Ar. The inset is the emission spectrum of $Ar_2^*$. Ionization potentials in the gas phase (upper) and in LAr (lower) for various molecules are also shown.

S. Suzuki, A. Hitachi, Charged Particles and Photon Interactions with Matter, CRC Press, Chapt. 31, (2011).

$$k = \sigma v$$

| System | $\tau_{ex}$ (s) | $k$ (cm$^3$/s) | $\sigma_{expt}$ (Å$^2$) | $\sigma_{d-d}$ (Å$^2$) | $T$ (K) |
|---|---|---|---|---|---|
| Ar*–Xe (s)[a] | $10^{-12}$ | $4 \times 10^{-8}$ | 100 (300) | 23 (35) | 20 |
| Ar*–Xe (s)[b] | $10^{-12}$ | $8 \times 10^{-9}$ | 30 (80) | 27 (40) | 10 |
| Ar*–Xe (l)[c] | $10^{-12}$ | $7 \times 10^{-9}$ | 10 (25) | 17 (26) | 90 |
| Xe*–C$_6$H$_6$ (s)[d] | $10^{-11}$ | $6 \times 10^{-8}$ | 100 (200) | 14 (21) [200][e] | 30–40 |

[a]Ophir *et al.* (Ref. 2); $k\tau_{ex} = 10^{-3}$ ppm$^{-1}$.
[b]Nanba *et al.* (Ref. 28) (see the text).
[c]Kubota *et al.* (Ref. 3).
[d]Ophir *et al.* (Ref. 2).
[e]The hard sphere collision cross section $\sigma_{HS}$ (see the text).

$$\sigma_{d-d} = 13.88 \left( \frac{\mu_A^2 \mu_B^2}{\hbar v \epsilon^2} \right)^{2/5} \qquad \sigma_{ph} = \frac{4\pi^2 E}{3\hbar c} \left( \frac{\mathscr{E}_{eff}}{\mathscr{E}} \right)^2 \frac{n}{\epsilon} \mu_B^2$$

dipole–dipole mechanism. The transfer probability $P_{d-d}$ due to dipole–dipole mechanism in the absence of diffusion is given by Dexter,[29]

$$P_{d-d} = \frac{3\hbar^4 c^4 Q_a}{4\pi R^6 n^4 \tau_s} \int \frac{F_s(E) F_a(E)}{E^4} dE = CR^{-6} , \qquad (3)$$

where $Q_a$ is integrated absorption cross section of acceptor, $R$ is the donor–acceptor separation, $\tau_s$ is the

$$k_{d-d}^D = 4\pi D\rho$$


Solid Ar–Xe (10K) Nanba et al. (1974)

Ar* + Xe → Ar + Xe$^+$          P.I.
Ar$_2$* + Xe → ArXe* + Ar      E.T.
ArXe* + Xe → Ar + Xe$_2$**
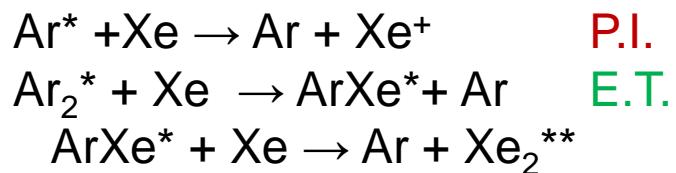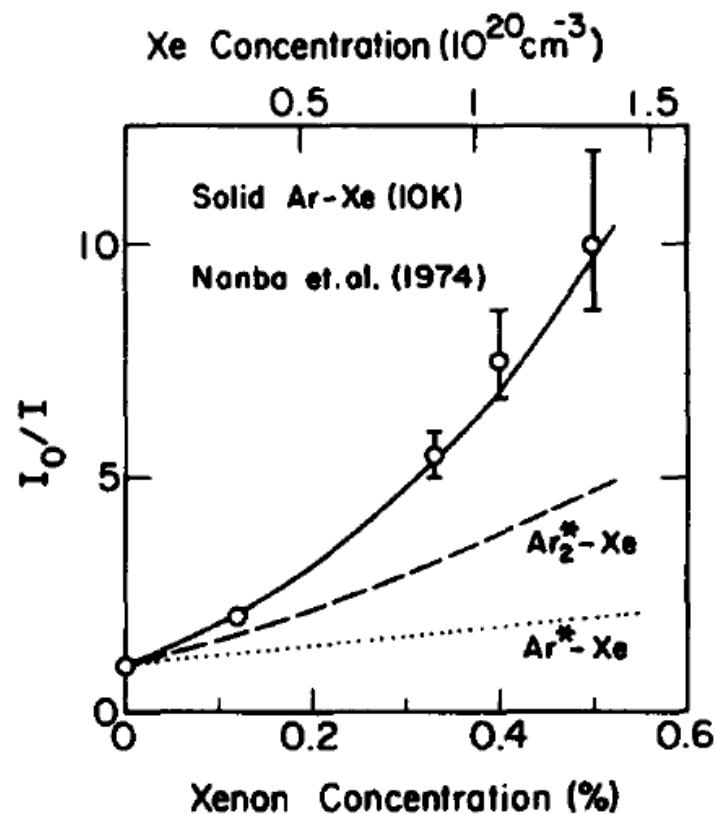
TABLE I. Ionization potential $IP$ in the gas phase and the estimated values of $I_s$ in liquid Ar and Xe for organic molecules used in the experiment. The values are in eV. The ion radii $r_+$ are in Å.

| Molecules | $IP$ | $r_+$ | $I_s$ in liquid Ar | $I_s$ in liquid Xe |
|---|---|---|---|---|
| Ethylene | 10.51 | 2.61 | 9.4 | 8.5 |
| Allene | 9.53 | 2.82 | 8.5 | 7.6 |
| Trimethylamine | 7.82 | 3.28 | 6.9 | 6.1 |
| Triethylamine | 7.50 | 3.81 | 6.7 | 5.9 |

$$I_s = IP + P_+ + V_0 \qquad P_+ = -\frac{e^2}{2r_+}(1 - \varepsilon^{-1})$$

# Photoionization

$Xe_2^* \rightarrow Xe + Xe + h\nu$ (vuv)

$h\nu + M \rightarrow M^+ + e^-$
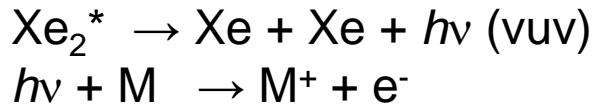
## Effective for heavy ions
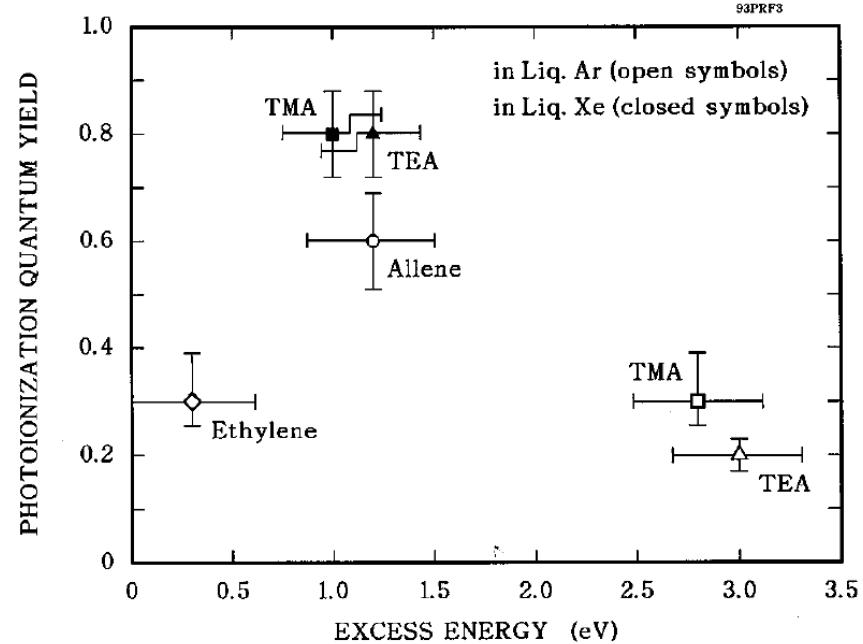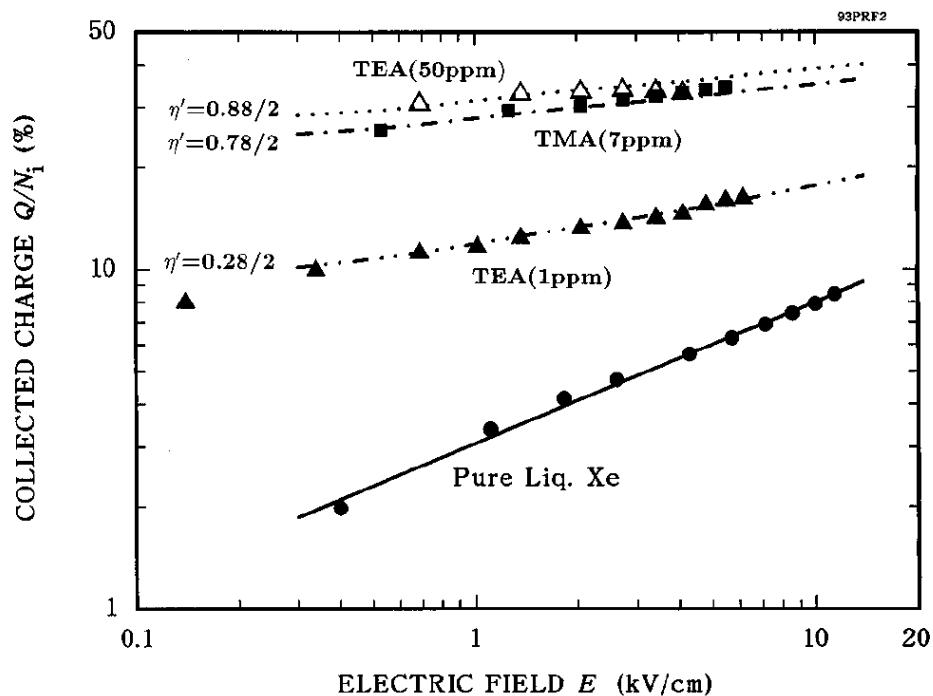


$$Q(E) = Q_\alpha(E) + \eta'[qN_i - Q_\alpha(E)]Y_{iso}(E) + \eta' qN_{ex}Y_{iso}(E)$$

$$\eta' = g\phi_{vuv}\phi$$

A. Hitachi et al. Phys. Rev. B 55, 5742 (1977)

# Field effects on quenching
## Recovery of quenching by electric field in LAr
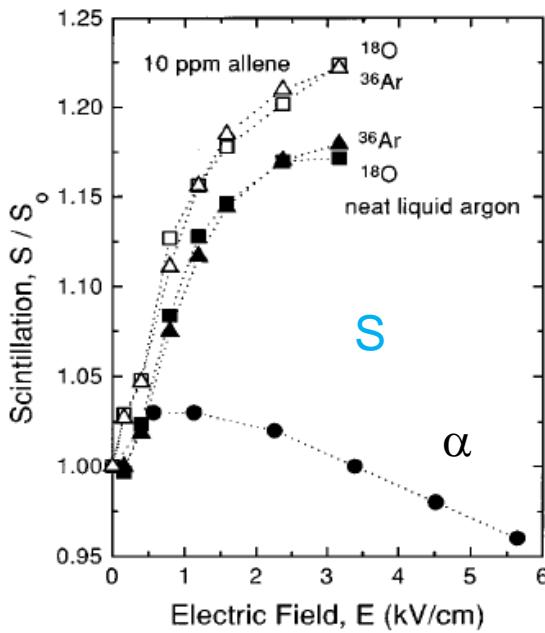


O  Ar

■  ▲  Pure Ar

□  △  allene doped
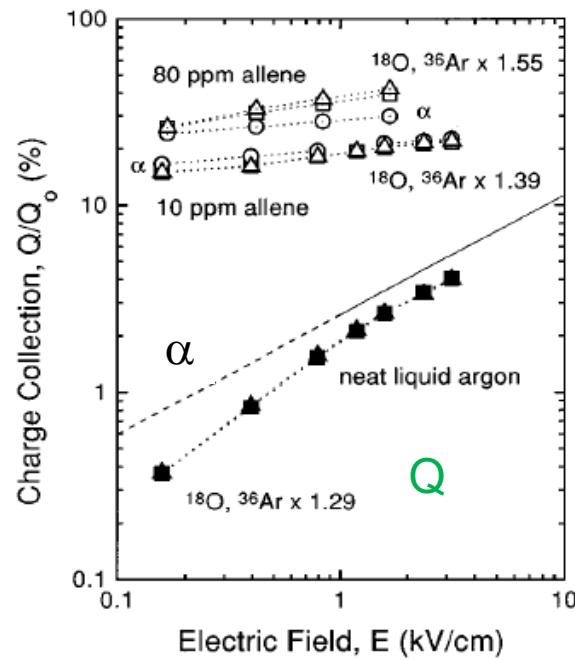
~30 MeV/n
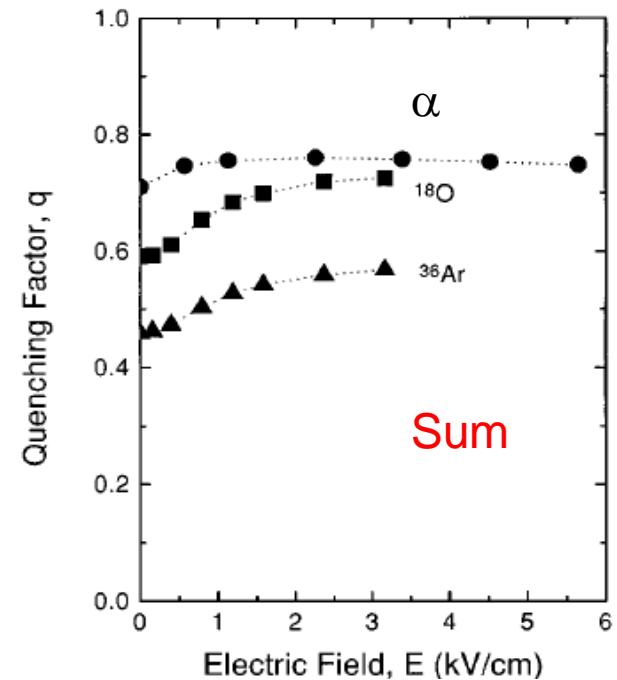
$q = q_0 S(E)/S_0 + [Q(E)/Q_0]/(1 + N_{ex}/N_i)$.

The recovery of quenching by **E** is observed, but limited, still $q < 1$

It has been reported for recoil Xe ions in LXe.

J.A. LaVerne et al. PRB 54, 15724 (1996)
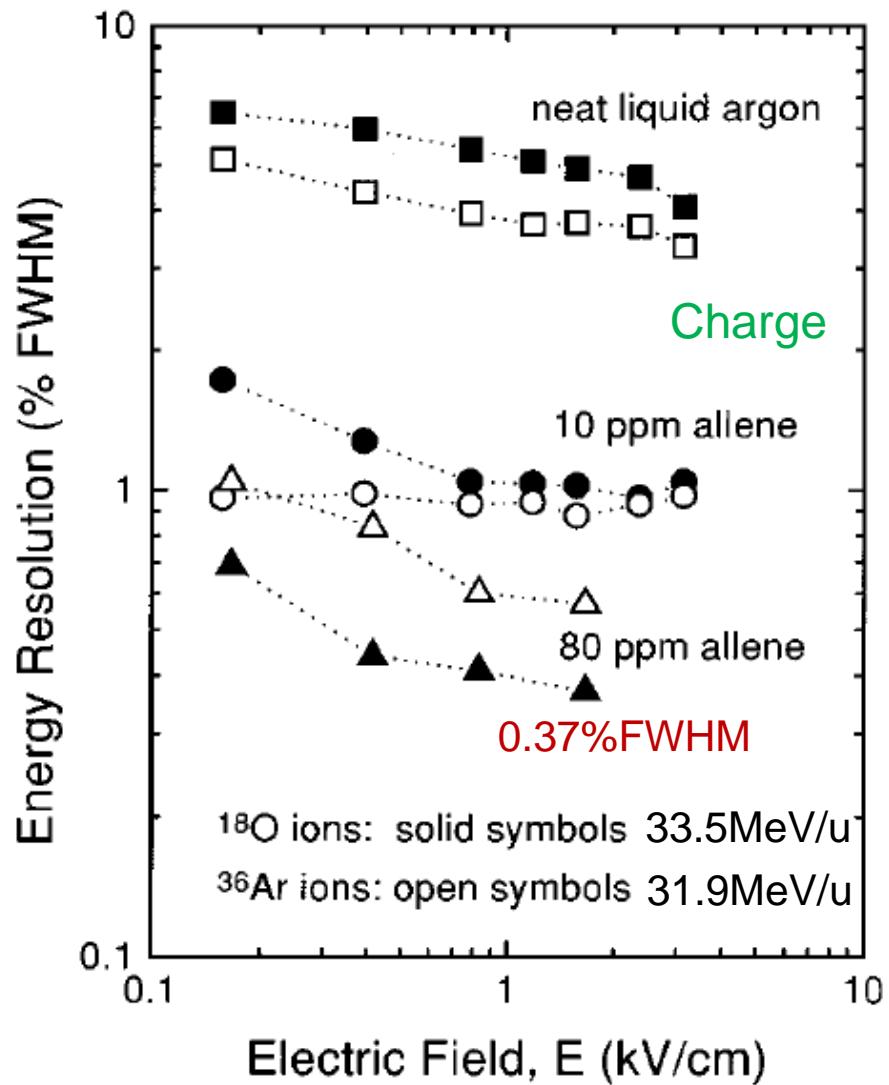
collected in this case was $10.0 \times 10^6$ electrons which gives a value for the FWHM of 0.075% assuming simple Poisson statistics with a Fano factor of 1. A close examination of the

LAr; Xe doping





$Ar_2^* + Xe + Xe \rightarrow Ar + Xe_2^{**}$
$Ar_2^* + Xe \rightarrow ArXe^* + Ar$
$ArXe^* + Xe \rightarrow Ar + Xe_2^{**}$

$Xe_2^{**} \rightarrow Xe_2^* + IR$
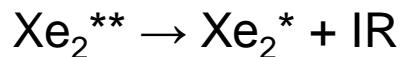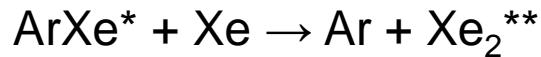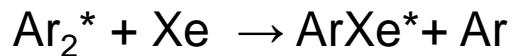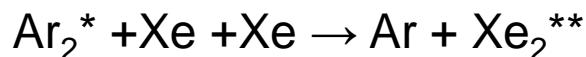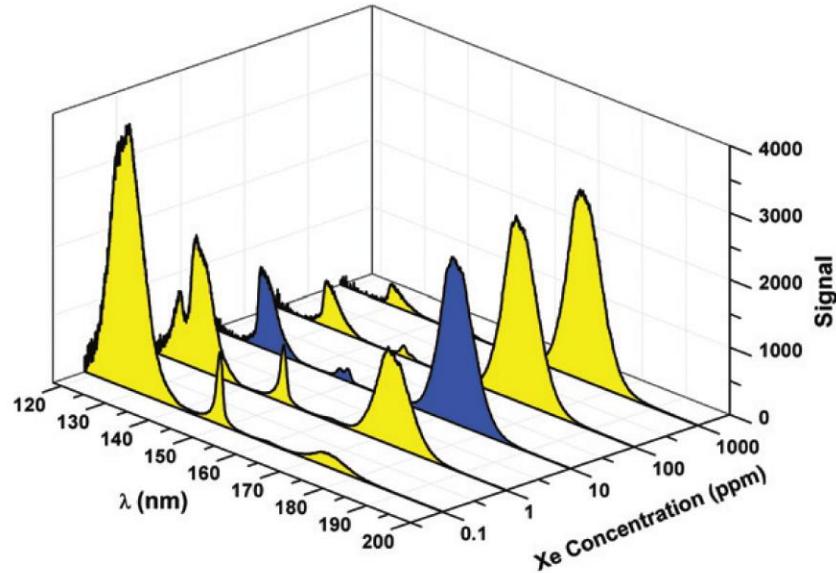
diffusion assisted, large rate $k$
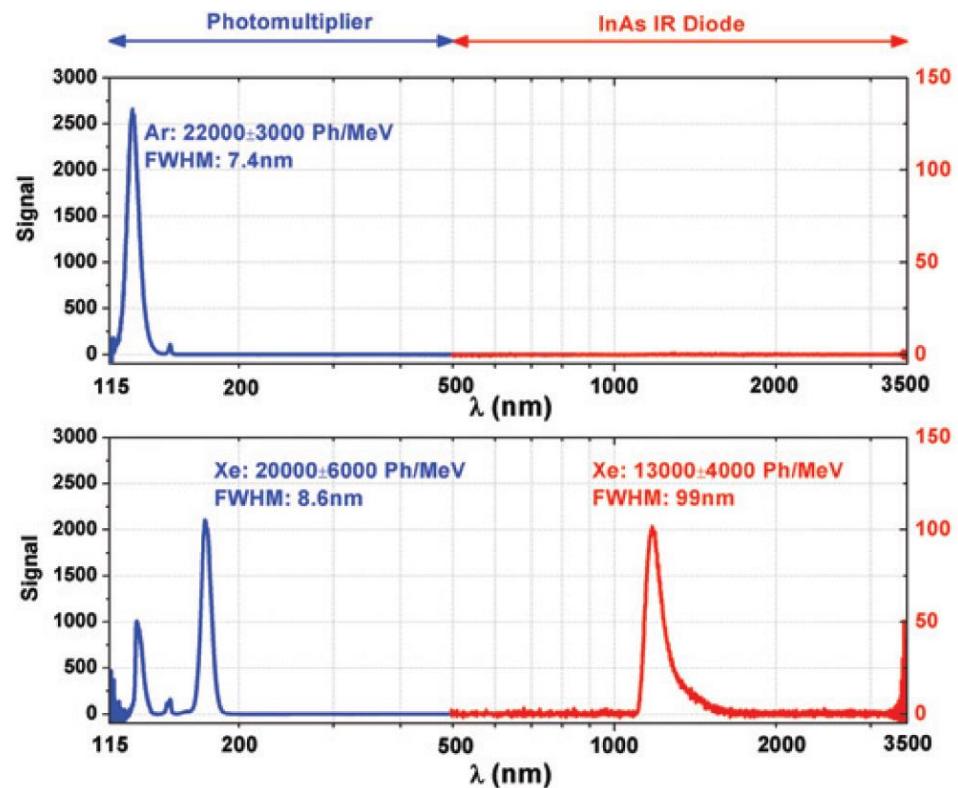
Heindl et al. Europhysics Letters 109, 12001 (2015)

# summary

I mean I stop here.
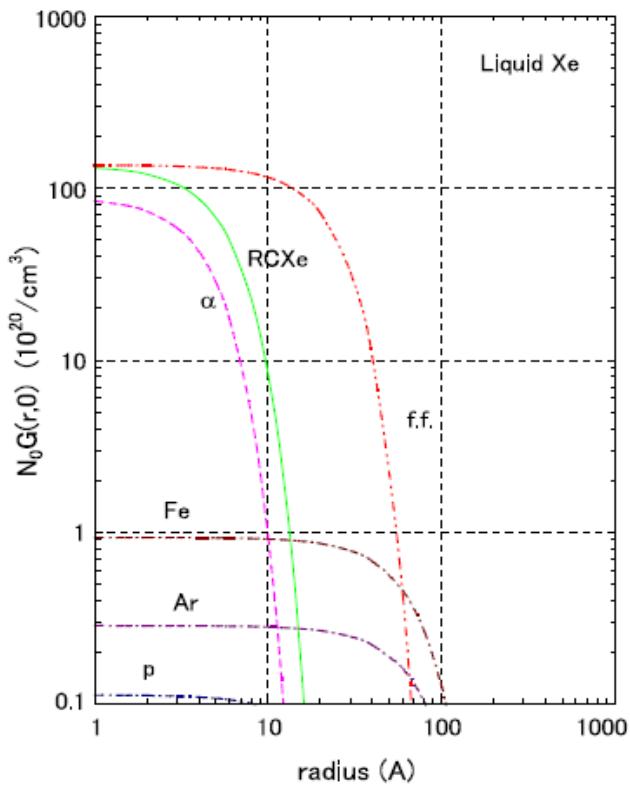
飛跡芯部の励起密度の半径依存性

Fig. 1. The initial radial distribution of excited species in the cylindrical track core in liquid Xe due to various ions. Solid curve shows 60 keV recoil Xe ions. Proton is 38 MeV and, Ar and Fe ions are relativistic.

反跳核は外部電場の影響を受け易い
　飛跡(芯)が単純な円筒状ではない
　飛跡が短い

$$R_2^* \rightarrow R + R + h\nu$$

$$R^* + R^* \rightarrow R + R^+ + e^- \; (KE)$$
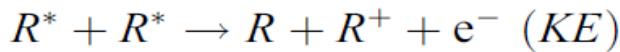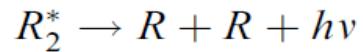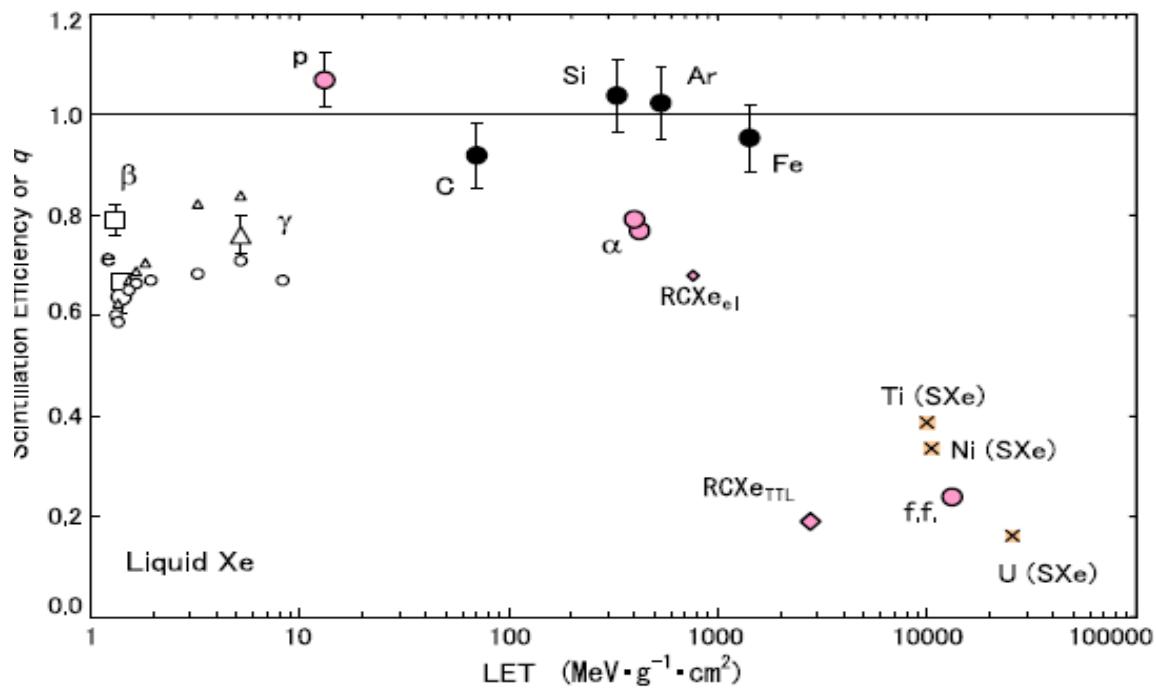
$$T_s = qT = q_c T_c + T_p$$

$$\partial n_1 / \partial t = D_1 \nabla^2 n_1 - k_1 n_1^2 - n_1 / \tau_1$$

$$\partial n_2 / \partial t = n_1 / \tau_1 - A_2 n_2$$

# liquid Ar
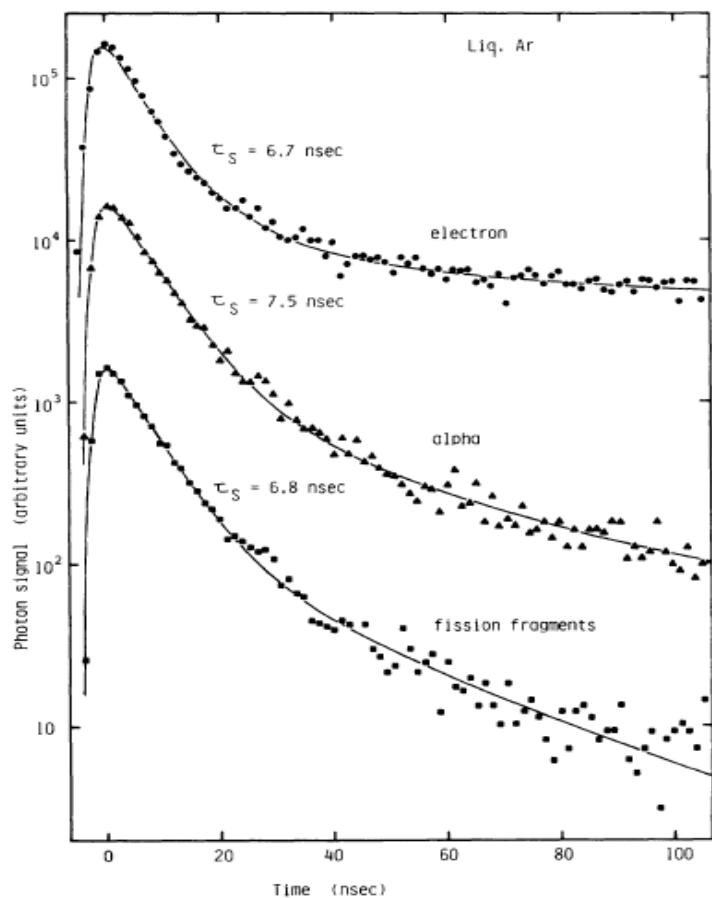


FIG. 2. Typical decay curves obtained for the luminescence from liquid argon excited by electrons (●), α particles (▲), and fission fragments (■) shown for the short time range. A slightly slow rise for electron excitation may be due to the recombination.
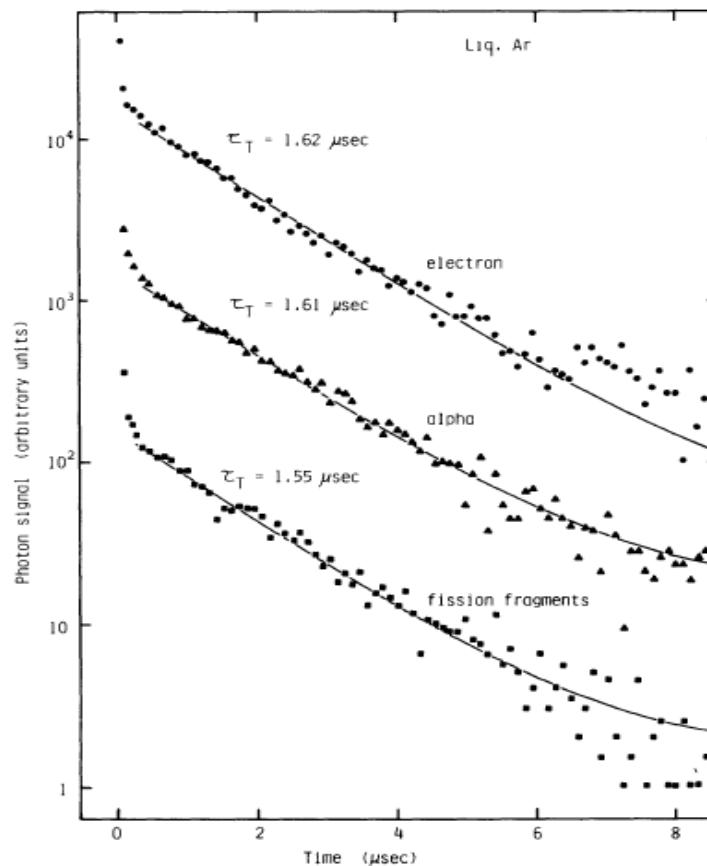
FIG. 3. Typical decay curves obtained for the luminescence from liquid argon excited by electrons (●), α particles (▲), and fission fragments (■) shown for the long time range. The fast exponential decay component is not shown in the figure.

# The refractive index of liquid and solid xenon

The refractive index **n** of an isotropic dielectric medium is in general complex and satisfies the dispersion relation[23]

$$\frac{\mathbf{n}^2 - 1}{\mathbf{n}^2 + 2} = \frac{4\pi Ne^2}{3m} \sum_i \frac{f_i}{\omega_i^2 - \omega^2 - i\Gamma_i\omega}, \tag{4}$$

where $\omega_i^2 - \omega^2$ is large compared with the term $\Gamma_i\omega$, the real part of the refractive index, $n$, can be approximated with

$$\frac{n^2 - 1}{n^2 + 2} \approx \frac{4\pi Ne^2}{3m} \sum_i \frac{f_i}{\omega_i^2 - \omega^2}. \tag{5}$$

The absorption spectra in condensed xenon show lines for Wanner-type "free" excitons. We replaced $\lambda_1$ and $\lambda_2$ by two major exciton lines of liquid xenon.

$$\frac{n^2 - 1}{n^2 + 2} = 1.2055 \times 10^{-2} \frac{2}{3} \frac{N_l}{N_g} \left( \frac{0.267\,83}{43.741 - \lambda^{-2}} \right.$$

$$\left. + \frac{0.294\,81}{57.480 - \lambda^{-2}} + \frac{5.0333}{112.74 - \lambda^{-2}} \right). \tag{8}$$

# 電場依存性

RN/$\gamma$比は、$\gamma$線の発光効率をYとおくと

$$\frac{\text{RN}}{\gamma} = \frac{q_\text{T}}{Y} = \frac{q_\text{nc} \cdot q_\text{e1}}{Y}$$

核的消光因子　　　　$q_\text{nc}$　　電場依存性なし
電子的消光因子　　　$q_\text{el}$　　電場依存性あり

再結合理論・発光効率理論
　Onsager　　　　　　低LET　　孤立系
　Jaffee　　　　　　　高LET　　均質系　$\mu_+ \sim \mu_-$
現象論
　Berks　　　　　　　中・高LET　有機シンチレータ
　Thomas-Imel　　　低・中LET

希ガス液体はいずれでも説明しきれない。
　熱電子化時間が非常に長い　　~ 1ns (LXe)
　熱電子化距離が非常に長い
　伝道帯があり電子移動速度が速い
　動的モデルが必要
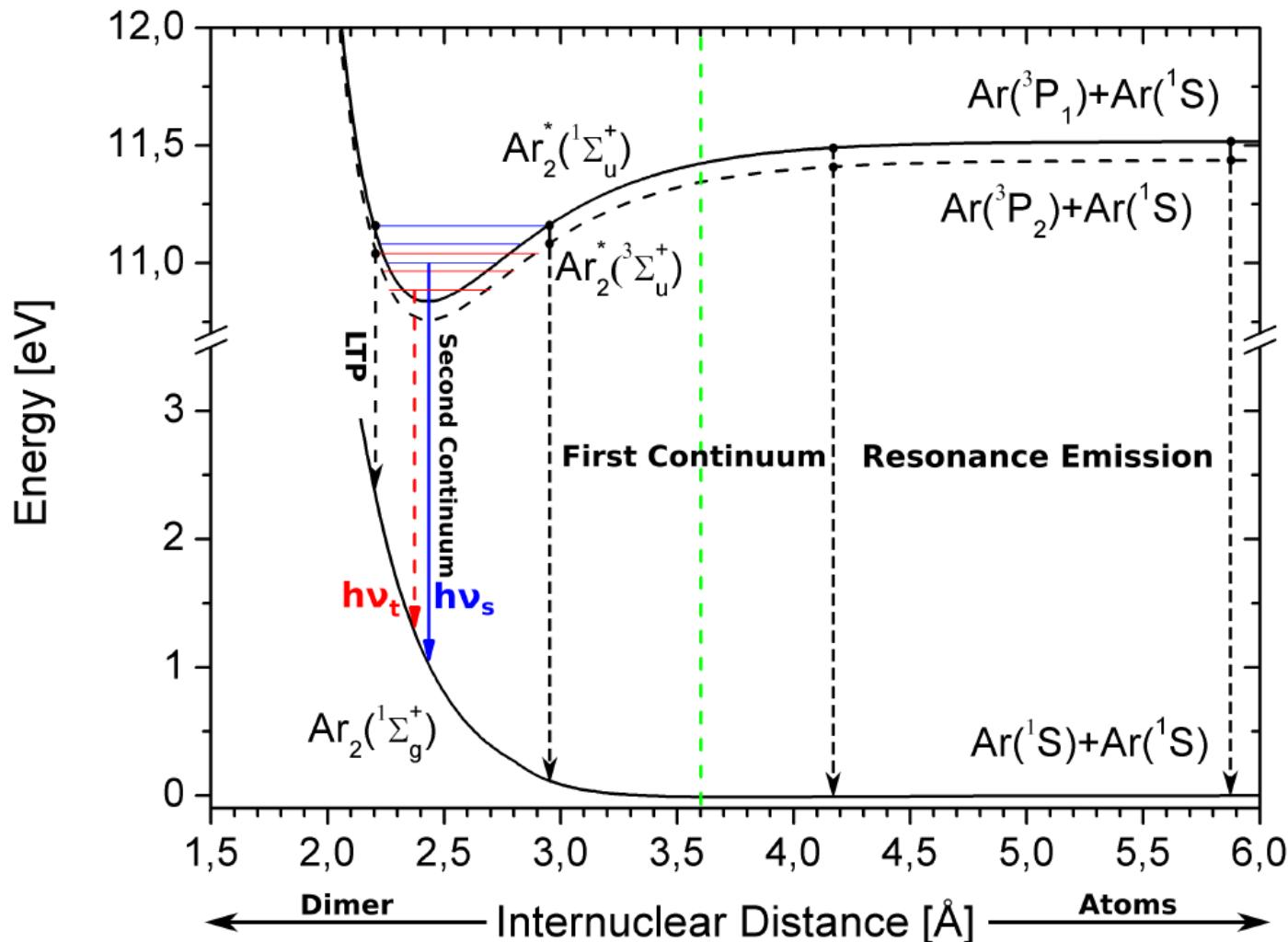
A. Neumeier, JAPS-Scintillation in Liquid Noble Gases